

# Effect of thickness on the physical properties and gas sensing application: anatase titanium dioxide nanofilms by automated nebulizer spray pyrolysis (ANSP)

V. Gopala Krishnan<sup>1,2</sup> · A. Purushothaman<sup>2</sup> · P. Elango<sup>1</sup>

Received: 20 February 2017 / Accepted: 10 April 2017  
© Springer Science+Business Media New York 2017

**Abstract** In this work, effects of thickness towards volume proportion of TiO<sub>2</sub> nanofilms were deposited on a glass substrate at 500 °C by using ANSP method. The optical profilometer shows the coated films thicknesses were increased (186, 234, 311, 397 and 433 nm) by increasing the volume proportion. Based on the thickness, The XRD reveals a polycrystalline tetragonal anatase phase with decreased particle sizes. The topographical study (AFM) of 3D surface view shows the incremented average roughness ( $R_a$ ) values. The surface morphological variations with decremented particle size were examined by FESEM. The maximum transmittance ~78.5% ( $\lambda = 612.8$  nm) is obtained to 186 nm thickness and further increment of thickness shows the decremented value of transmittance with an absorption edge shifted from lower to higher wavelength (blue shift) and the calculated band gap value  $E_g = 3.65$ – $3.26$  eV. The gas sensing performances of films was studied by using a various sensing parameters, obviously C<sub>2</sub>H<sub>6</sub>O gas shows highest response ( $S_m = 13\%$  as 397 nm) at 300 °C for 150 ppm gas concentration against other gasses (NH<sub>3</sub>, CH<sub>4</sub>O, C<sub>3</sub>H<sub>8</sub>O and C<sub>3</sub>H<sub>6</sub>O).

## 1 Introduction

The improvement of nanoscience and nanotechnology plays an effective role to reduce several global environmental

problems such as the greenhouse effect and the ozone hole. These problems are related to the release of pollutant gasses in the atmosphere, therefore their exposure and demolitions are the hot global priority. As mentioned in the literature, the semiconducting metal oxide of solid-state (SnO<sub>2</sub>, TiO<sub>2</sub>, ZnO) gas sensors is widely preferred due to a sequence of specific advantages [1]. Particularly, *n*-type metal oxide semiconductor of titanium dioxide (TiO<sub>2</sub>) is an effective material for the different new applications such as solar cell [2], purifier of environmental pollutants [3], photocatalysis [4], gas sensors [5], corrosion-protection [6] and microelectronics [7, 8] applications, due to its properties of non-toxicity in aqua, reasonable cost, powerful oxidation potential and high chemical inertness TiO<sub>2</sub> is an attractive material owing to their notable ability to change the electrical resistance (conductance) in response to oxidizing and reducing gasses, and the electronic structure of TiO<sub>2</sub> and its consequences as far as the gas sensing performance is concerned immensely.

TiO<sub>2</sub> defined with three polymorphic forms such as anatase, brookite, and rutile. The Rutile ( $D_{4h}$ , <sup>14</sup>P4<sub>2</sub>/mm, symmetry) and anatase ( $D_{4h}$ , <sup>19</sup>I4<sub>1</sub>/amd, symmetry) make a tetragonal phase and they were developed commercially, but the orthorhombic phase of brookite (Pcab, lower symmetry) is very difficult to prepare but naturally present in a solitary crystal form. Brookite and anatase may be turned to rutile phase by the subject of higher temperature, usually at ~750 to ~1000 °C respectively [9]. A rutile phase is usually the dominant phase in TiO<sub>2</sub>, but some work has been synthesizing an anatase phase because of their importance in practical engineering applications in sensors [10]. The fabrication of the anatase and rutile phases strongly depends on the temperature and deposition method [11]. Attentively many techniques are used to prepare the stabilized anatase TiO<sub>2</sub> thin films namely, sol–gel [12], chemical

✉ P. Elango  
yuvagopal@yahoo.in

<sup>1</sup> Department of Physics, Government Arts College,  
Coimbatore 641018, India

<sup>2</sup> Department of Physics, Sree Sakthi Engineering College,  
Coimbatore 641104, India

vapor deposition [13], pulsed laser deposition [14], electrochemical [15], RF-magnetron sputtering and spray pyrolysis deposition [16]. Among them, the spray pyrolysis is one of the significant methods which may effectively open new routes to nanotechnology. This process importantly has a very safety, less expensive, no need in vacuum arrangement and sustaining homogeneity in large area of film coating [17] behaviors.

Significantly, the effect of thickness plays an important role in controlling the phase stability and film properties, which is one of the critical parameters to achieve a desired structural and functional property [18]. As our knowledge, only a few works have been studied by using acetylacetonone stabilized Ti-alkoxide precursors, whereas the phase stability was not maintained on their works also [19–21]. Particularly no systematic study of structural and optical characterization of the anatase phase TiO<sub>2</sub> films deposited by spray pyrolysis technique from the source of acetylacetonone stabilized Ti-isopropoxide have been performed. Predominantly, the automated nebulizer sprayed anatase phase stabilized and gas sensing performances of TiO<sub>2</sub> film have not been studied so far. The aim of this work is to deposit TiO<sub>2</sub> nanofilms on preheated glass substrate at 500 °C with different volume proportions by the method of automated nebulizer spray pyrolysis and exemplify the effect thickness on structural, optical, topography, morphological and gas sensing performance of TiO<sub>2</sub> nanofilms.

## 2 Experimental details

TiO<sub>2</sub> nanofilms array with nominal volume proportions (x) of 2.5, 5.0, 7.5, 10.0 and 12.5 ml is taken and prepared by using automated nebulizer spray pyrolysis technique (ANSP) in an air atmosphere. The experimental setup, procedure and advantages of ANSP were explained [9] elsewhere and the observed basic parameters were mentioned in Table 1. The primary stock solution was prepared with 0.1 M/l of titanium tetra-isopropoxide (TTIP) [Ti[OCH(CH<sub>3</sub>)<sub>2</sub>]<sub>4</sub>] dissolved in 50 ml mixed solution of ethanol (EtOH) (C<sub>2</sub>H<sub>5</sub>OH) solvent with acetylacetonone (AcAc) [CH<sub>3</sub>COCH<sub>2</sub>COCH<sub>3</sub>] stabilizer in the ratio of (4:1) and stirred for 15 min by using magnetic stirrer. The obtained transparent pale yellow solution with different above mentioned volume proportions was sprayed on the ultrasonically cleaned glass substrate at 500 °C.

Various volume proportions of coated films may bring into being a various thickness of the films and their characterization is analyzed by the following study. The structural properties of TiO<sub>2</sub> films were entirely studied by X-ray diffraction (Bruker D8 advance X-ray diffractometer) with Cu K $\alpha$  radiation ( $\lambda=0.15418$  nm). Surface morphology of the films was characterized via atomic force microscope

**Table 1** Optimized spray parameter for TiO<sub>2</sub> nanofilms with thickness variation

Particulars	Parameter
Spray type	Nebulizer
Air blast	Atomizer
Carrier gas pressure	30 Pa
Solution flow rate	0.10 ml/min
Distance from substrate to spray nozzle	5 cm
Substrate type	Glass
Solvent	Ethanol and acetyl acetone
Precursor	Titanium isopropoxide
Concentration	0.1 mol/l
Deposition variation	2.50, 5.00, 7.50, 10.00, 12.50 ml
Deposition temperature	500 °C

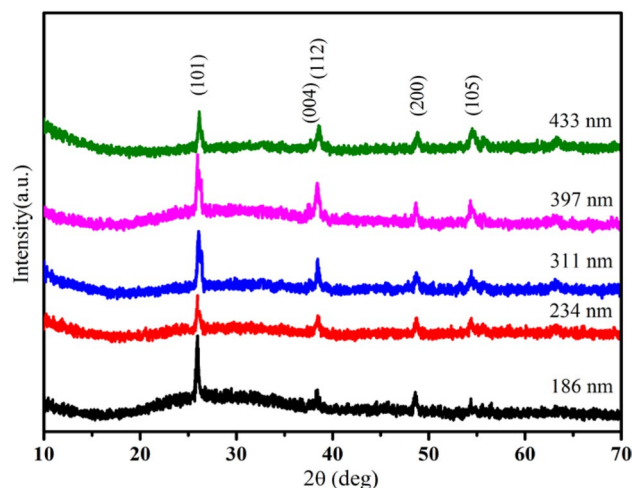


**Fig. 1** XRD study on various thickness of TiO<sub>2</sub> nanofilms

(AFM, Model-Nanoscope E) and field emission scanning electron microscopy (FESEM, Quanta-250 FEG) applying an operating voltage 30.0 kV. An optical study of the films was done by Ultra Violet–Visible–Near Infrared (UV–Vis–NIR) spectrophotometer (Model JASCO-V-500) in the range from 250 to 980 nm and thickness of the films was determined by using surface profilometer (SJ-301 Mitutoyo). Finally, the gas sensing performances were studied by LCR meter (GW Instek LCR-821).

## 3 Results and discussion

XRD study of thickness varied (186, 234, 311, 397, 433 nm) nanofilms of TiO<sub>2</sub> are shown in Fig. 1. The coated films were generally polycrystalline with stabilized anatase form of tetragonal phase with prominent diffraction peaks

at  $2\theta = 25.51, 38.31, 48.66$  and  $55.44^\circ$  corresponding to (101), (112), (200) and (105) reflection planes were well fitted with standard JCPDS data, card no. 89-4921. Mean-time, this film was not detected other two remaining phases (brookite, rutile) because the preparation method and raw materials were maintain the phase stability [22]. The crystallite size 'D' is calculated using Scherrer formula [23],

$$D = \frac{0.9 \times \lambda}{(\beta \times \cos \theta)} \quad (1)$$

$$d = \frac{n\lambda}{(2 \sin \theta)} \quad (2)$$

where D is the crystalline size,  $\lambda$  is the wavelength of X-rays,  $\beta$  is the broadening of diffraction line measured at half its maximum intensity in radius, d is interplaner spacing value and  $\theta$  is the angle of diffraction. The average crystallite size and d-spacing value were found to decrease with increase in thickness and their intensity of TiO<sub>2</sub> films varied with respect to thickness. The lattice constants determined from the present data are  $a = 3.788$  and  $c = 9.549 \text{ \AA}$ . The dislocation density and microstrain were calculated by using equations (3) and (4) for TiO<sub>2</sub> films [9].

$$\delta = \frac{1}{D^2} \quad (3)$$

$$\epsilon = \frac{\lambda}{D \sin \theta} - \frac{\beta}{\tan \theta} \quad (4)$$

The variation of dislocation density and microstrain with different thickness of TiO<sub>2</sub> was listed in Table 2. It has been confirmed that the calculated average crystalline size, d-spacing value, lattice parameter, dislocation density and microstrain of the obtained films values corresponded to that of the bulk TiO<sub>2</sub> anatase phase structure [24].

Atomic force microscope (AFM) allows us to get microscopic information on the surface structure and to plot topographies representing the surface relief. This technique offers digital images which allow quantitative measurements of surface features, such as root mean square roughness  $R_q$ , or average roughness  $R_a$ , and the analysis of images from different perspectives, including three-dimensional simulation. The topography view of  $2 \mu\text{m} \times 2 \mu\text{m}$  sized three-dimensional AFM images of TiO<sub>2</sub> nanofilms with different thickness (186, 234, 311, 397, 433 nm) is shown in Fig. 2a–e. In sample with the lowest thickness, particles rather are isolated from each other (Fig. 2a, b) while in Fig. 2c–e are continually in distribution these changes in surface morphology might lead to degradation in the crystalline quality of the film [25]. This suggests that the particles seen at the surface of the film are clusters of crystallites. The AFM analyses of average roughness parameters were listed in Table 2. It can be seen from the figure, the surface roughness and coating thickness of

the films is increased with respect to thickness. This variation shows the fine correspondence with crystalline size and d-spacing value of XRD study. Figure 2f–j shows the surface morphological characterisation of TiO<sub>2</sub> nanofilms and it is analysed by using field emission scanning electron microscope (FESEM). The smaller thickness of the coated films (186 nm) depicts the spherical shape structures and for the thickness of 234, 311, 397, 433 nm shows the micro spherical structures. The observed particle sizes were decreased by increase in thickness, which is in good agreement with structural and topography study.

The optical transmittance spectra of TiO<sub>2</sub> nanofilms over the spectral range of 250 nm to 980 nm are shown in Fig. 3. The oscillating nature of average transmittance is enhanced up to 78.4% (at  $\lambda = 616 \text{ nm}$ ) for the coated film of 186 nm thickness. The transmittance values of all coated films were decreased by increase in thickness. This decrement is caused by the fundamental absorption of light may increase the quality of defect less films immensely [26]. The UV region of sharp absorption edges was shift from shorter to longer wavelength (Blue-shift) due to the thickness (186, 234, 311, 397, 433 nm) variations, since the improvement in crystal quality of the films along with a reduction in porosity [27]. The band gap energy was calculated by using the Tauc's relation [28].

$$\alpha(h\nu) = A(h\nu - E_g)^{1/2} \quad (5)$$

where  $E_g$  is the optical band gap of the sample and A is constant. Optical band gap ( $E_g$ ) energy of TiO<sub>2</sub> film is carried out by extrapolating linear region spectrum  $(\alpha h\nu)^2$  versus  $(h\nu)$  as shown in Fig. 4. The obtained band gap energy ( $E_g = 3.26\text{--}3.65$ ) is decreased from higher to lower with respect to increasing thickness because of an improvement in film quality may reduce the structural defect. The standard band gap energy of anatase phase TiO<sub>2</sub> is 3.20 eV is finely coinciding with a coated thickness of 397 nm, hence the film was currently matched with XRD study.

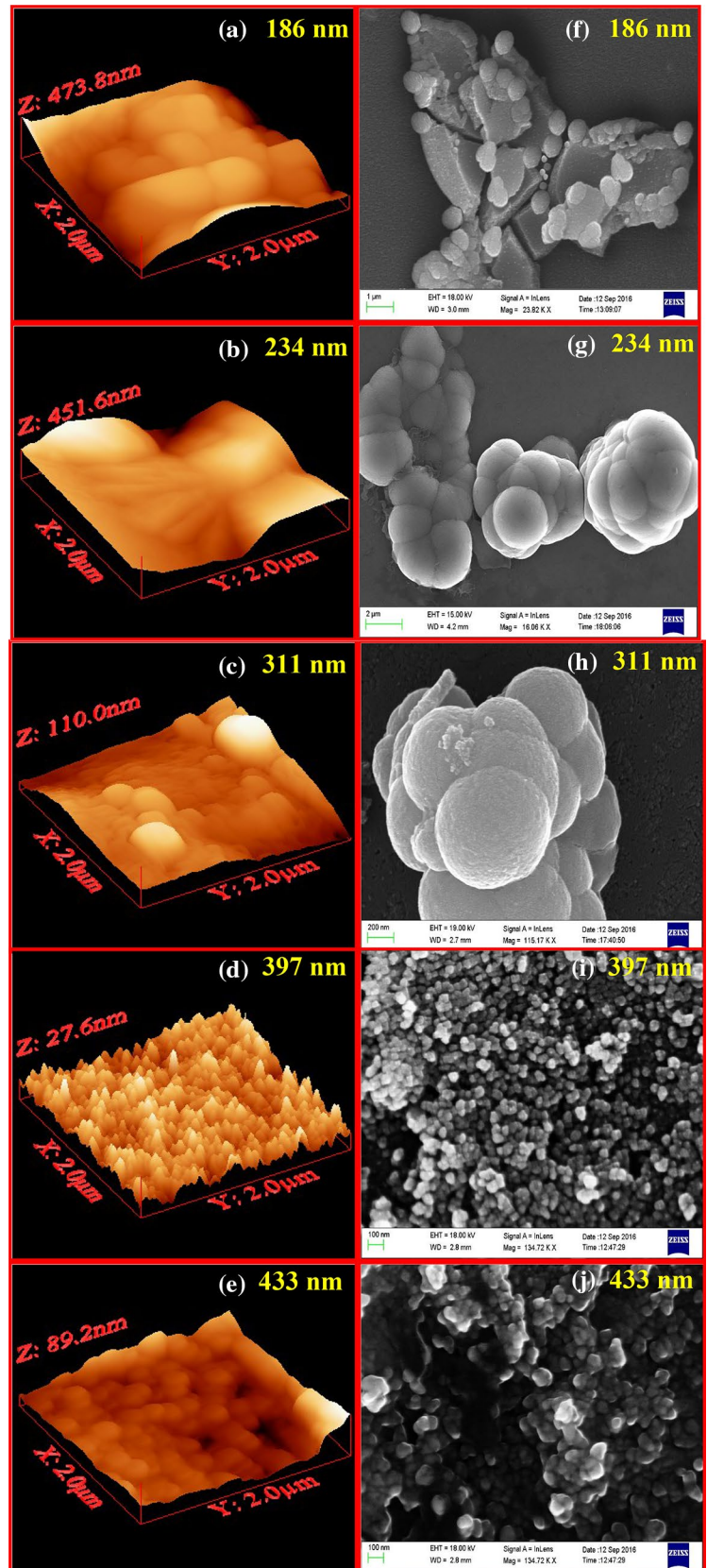
### 3.1 Gas sensing behavior of TiO<sub>2</sub> nanofilms

The schematic diagram of the gas sensor setup was represented in Fig. 5. As we can be seen, the cylindrical stainless steel testing chamber inbuilt with a nichrome-heating element and a chromel–alumel thermocouple is fixed at bottom of the testing chamber and it is well connected with a temperature controller for adjusting the temperature (~up to 500 °C). The sensing measurements were proceeded by a static process: a specified amount of the test gas such as C<sub>2</sub>H<sub>6</sub>O, NH<sub>3</sub>, CH<sub>4</sub>O, C<sub>3</sub>H<sub>8</sub>O, and C<sub>3</sub>H<sub>6</sub>O was injected into a testing chamber and mixed with air. A mass flow controller (MFCs) was used to control the concentration of the test gasses. The sensor films were electrically connected to a

**Table 2** Obtained values of structural parameters, average roughness and coating thickness of the TiO<sub>2</sub> films

Volume (ml)	Peak position 2θ (deg)	FWHM value (deg)	(h k l)			"D" partical size (nm)	"g" dislocation ×10 <sup>14</sup> (linmet <sup>-2</sup> )	"g" strain ×10 <sup>4</sup> (lin <sup>-2</sup> met <sup>-4</sup> )	"d spacing" value ×10 <sup>-10</sup> m	Stacking fault	Average roughness (nm)	Thickness (nm)
			h	k	l							
2.50	25.930	0.1673	1	0	1	50.94	3.854	7.114	3.436	0.088	1.781	186
	38.313	0.2007	0	0	4	43.80	5.212	8.272	2.349	0.086		
	48.621	0.2676	2	0	0	34.05	8.624	10.641	1.873	0.101		
	54.364	0.8029	1	0	5	11.63	73.973	31.164	1.688	0.283		
	25.832	0.1673	1	0	1	50.93	3.856	7.115	3.449	0.088	2.061	234
5.00	38.454	0.4015	0	0	4	21.90	20.841	16.542	2.341	0.172		
	48.130	0.2676	2	0	0	33.99	8.657	10.661	1.891	0.101		
	54.400	0.4015	1	0	5	23.25	18.492	15.581	1.687	0.142		
	25.703	0.2007	1	0	1	42.44	5.552	8.538	3.466	0.106	2.683	311
	38.459	0.3346	0	0	4	26.28	14.474	13.785	2.341	0.143		
10.00	48.458	0.3346	2	0	0	27.22	13.501	13.314	1.879	0.126		
	54.153	0.5353	1	0	5	17.42	32.943	20.797	1.694	0.189		
	25.387	0.2676	1	0	1	31.81	9.883	11.391	3.508	0.143	2.815	397
	37.872	0.2342	0	0	4	37.49	7.116	9.666	2.376	0.101		
	48.146	0.4725	2	0	0	19.25	26.988	18.824	1.890	0.179		
12.50	53.153	0.4015	1	0	5	23.13	18.697	15.668	1.723	0.144		
	25.197	0.2007	1	0	1	42.40	5.563	8.546	3.534	0.107	3.104	433
	37.912	0.4684	0	0	4	18.75	28.458	19.329	2.373	0.202		
	48.082	0.3346	2	0	0	27.18	13.541	13.333	1.892	0.127		
	53.225	0.6022	1	0	5	15.42	42.035	23.492	1.721	0.215		

**Fig. 2** a–j Topography view of AFM and surface morphology of FESEM for TiO<sub>2</sub> thin films



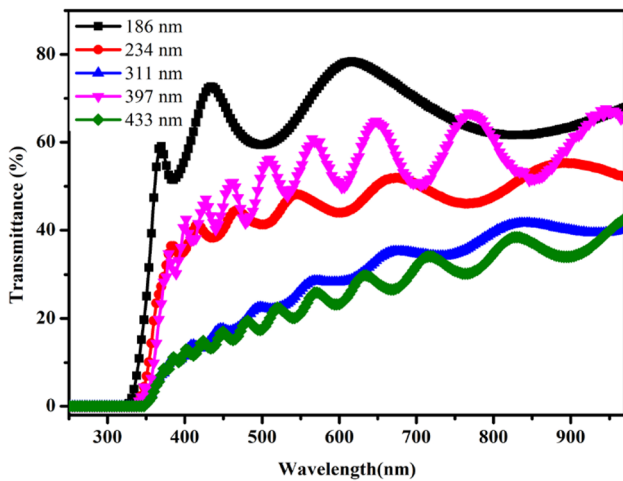


**Fig. 3** Variation of transmittance as a function of wavelength for TiO<sub>2</sub> nanofilms

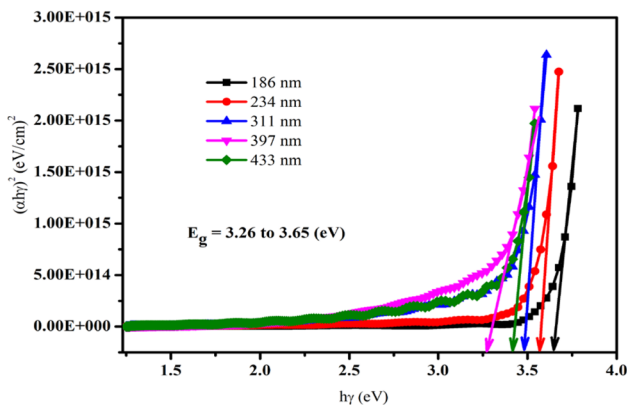


**Fig. 4** Plot of  $(\alpha h\nu)^2$  versus  $h\nu$  for TiO<sub>2</sub> films sprayed at 773 K

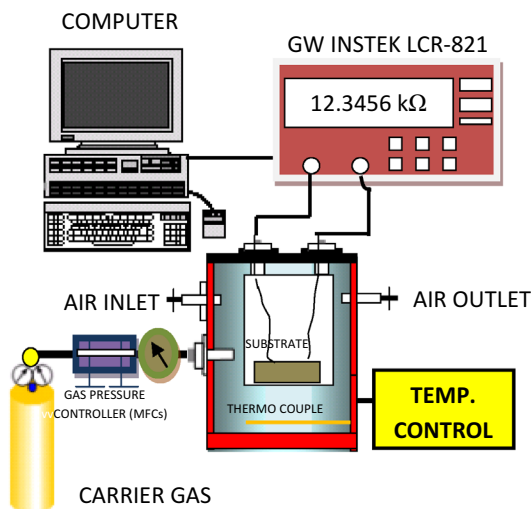


**Fig. 5** Schematic diagram of gas sensor setup

two-probe setup for measure the resistance variation (GW Instek LCR-821) and hence calculate the sensing response. The gas sensitivity response (*S*) factor of TiO<sub>2</sub> nanofilms was calculated by using the relation of resistance in the air (*R*<sub>air</sub>) and resistance in reducing gasses (*R*<sub>gas</sub>), which was expressed as [29].

$$S = \frac{R_{air} - R_{gas}}{R_{gas}} = \frac{\Delta R}{R_{gas}} \sim \frac{R_{air}}{R_{gas}} \quad (6)$$

Based on that, various parameters such as crystallite size, film thickness, porosity, amount and nature of dopant, catalysts and surface states are known to be important in enhance the gas sensitivity of the sensors element [30]. The main emphasis of this letter is to study the chemiresistors (metal oxide) gas sensing surface phenomenon of adsorbed oxygen and different gases (CH<sub>3</sub>OH, NH<sub>3</sub>, C<sub>3</sub>H<sub>8</sub>O, C<sub>2</sub>H<sub>6</sub>O and C<sub>3</sub>H<sub>6</sub>O) with various parameters of sensitivity, selectivity, response and recovery times with respect to the function of temperature (°C) and gas concentration (ppm) of pure titanium oxide nanofilms were prepared by using automated nebulizer spray pyrolysis method. The sensing nature of pure TiO<sub>2</sub> films significantly relates with operating temperature [31]. Accordingly, the gas sensing response behaviour of various coated thickness (186, 234 nm, 311, 397, 433 nm) of TiO<sub>2</sub> nanofilms were represented with a function of temperature (50–350°C) at an constant gas concentration (150 ppm) of C<sub>2</sub>H<sub>6</sub>O reducing gas is shown in Fig. 6(left). As we can be seen, the gas response of all the films increased with respect to operating temperature, the sensor element (TiO<sub>2</sub>) of the various coated thickness of the films reaches the maximum gas response (*S*<sub>m</sub> = 13% as 397 nm) at 300°C and then falls with further increase in operating temperature is due to the mechanism of gas adsorption and desorption of chemiresistors (metal oxide) [1]. Similarly, Fig. 6(right) denote the various reducing gas sensing response of 397 nm thickness of TiO<sub>2</sub> with a function of temperature (50–350°C) at a constant gas concentration (150 ppm). Among the various reducing gas, the C<sub>2</sub>H<sub>6</sub>O reducing gas reveals the highest gas response (*S*<sub>m</sub> = 13%) may be due to the surface phenomenon of adsorbed oxygen, nanocrystalline nature of films and higher surface to volume ratio [32].

The dependence of sensitivity towards different thickness of (186, 234, 311, 397, 433 nm) TiO<sub>2</sub> on the C<sub>2</sub>H<sub>6</sub>O gas concentration at an operating temperature of 300°C is shown in Fig. 7(left). It is observed that the sensitivity increases linearly as the C<sub>2</sub>H<sub>6</sub>O concentration increases from 30 to 150 ppm and then decreases with further increase in the C<sub>2</sub>H<sub>6</sub>O gas concentration. The linear relationship between the sensitivity and the C<sub>2</sub>H<sub>6</sub>O gas concentration at low concentrations may be attributed to the availability of a sufficient number of sensing sites on the

film to act upon the  $C_2H_6O$ . The lower and higher gas concentration involves a lower and higher surface coverage of gas molecules, resulting in a lower and higher surface reaction between the surface adsorbed oxygen species and the gas molecules. Further increase in gas concentration the surface reaction will be gradual and reached saturation of the surface coverage of gas molecules. Thus, the maximum sensitivity was obtained at an operating temperature of  $300^\circ C$  for the exposure of 150 ppm of  $C_2H_6O$  reducing gas.

**Fig. 6** Sensitivity response of ethanol gas with the function of temperature for various coated thickness, sensitivity response to 397 nm thickness with an functions of temperature (right)

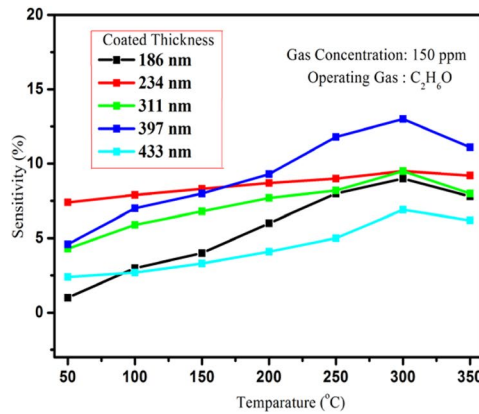
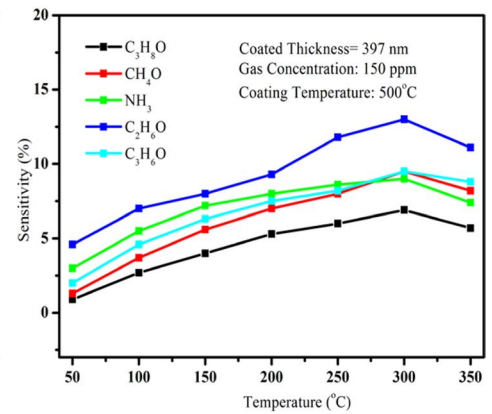
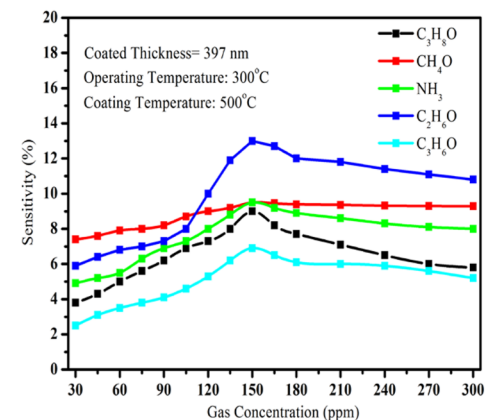
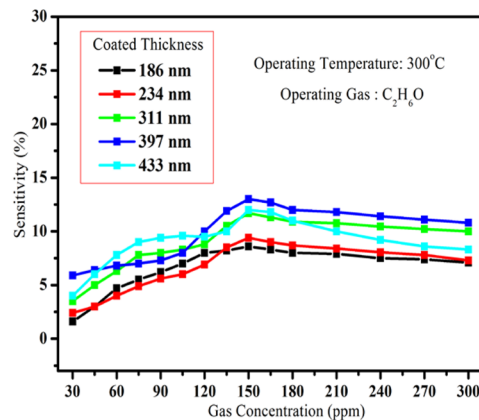


Figure 7(right) shows the various reducing gas response to 397 nm thickness of  $TiO_2$  films at  $300^\circ C$  operating temperature for different gas concentration. Which is shows the  $C_2H_6O$  gas exposes highest sensitivity response when compared with other reducing gasses.

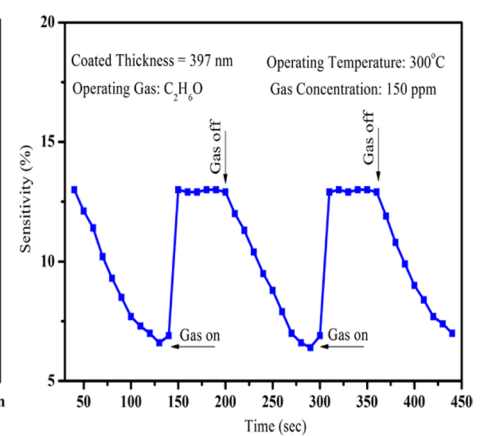
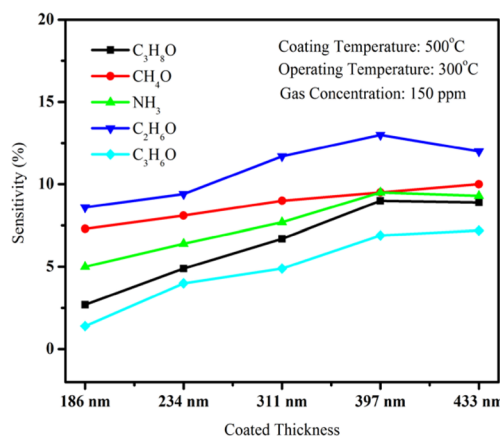
Figure 8(left) shows the sensitivity response to different thickness (186, 234, 311, 397, 433 nm) of various reducing gasses at  $300^\circ C$  operating temperature with constant gas concentration (150 ppm). Among all gasses, the  $C_2H_6O$



**Fig. 7** Sensitivity response of ethanol gas with the function of gas concentration for various coated thickness (left), sensitivity response to 397 nm thickness with an functions of gas concentration (right)



**Fig. 8** Sensitivity response of various gases with the function of coated thickness (left side), sensitivity response and recovery time to 397 nm coated film of  $TiO_2$  (right side)



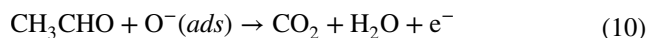
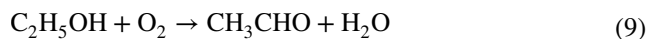
gas reveals the high sensitivity response for the respective parameter. The effective of these sensors is very fast as it can be observed; that the gas response and gas recovery times are defined as the times of conductance takes to reach 90% of  $(R_f - R_0)$  when the gas is introduced and to recover 30% of  $(R_f - R_0)$  when the flux of the air is restored. Figure 8(right) says the response and recovery time for  $C_2H_6O$  are about 20 and 90 s respectively. The quick response  $C_2H_6O$  gas may due to faster oxidation, which shows their good sensing ability and their time to the sensitivity response of the sensor element has approximately constant in every cycle, which is indicating the repeatability of the sensor.

### 3.2 Gas sensing mechanism

The fast response and quick recovery of  $C_2H_6O$  reducing gas having a most important feature of the present investigation are high gas response, high selectivity to against other gasses ( $NH_3$ ,  $CH_4O$ ,  $C_3H_8O$ , and  $C_3H_6O$ ). The enhanced response could be attributed to nanocrystalline nature of the films. It is known that the high sensitivity performances were sustained with a metal oxide, which absorbs oxygen species of  $O^{-2}$ ,  $O^{-}$  or  $O^{2-}$  from the surrounding and also control the increment of conductivity due to electron capture by oxidizing gas [33] were as,



The presence of chemically adsorbed oxygen could cause electron depletion in the thin film surface and be building up of Schottky surface barrier; consequently, the electrical conduction of thin film decreased to a minimum. When a surface of the material exposed to the reducing gas, the interaction with the chemisorbed oxygen can take place in a various way. Here, the maximum sensitivity of surface reactions can be written to the reducing gas of ethanol as the follows [34]:



with this reaction, many electrons could be released to a thin film surface. This could make the Schottky surface barrier decrease; with the depletion layer thinner; consequently, the electrical conductance of the thin film increases. More gas would be absorbed by the thin film surface; thus, the gas sensitivity was enhanced. An increase in operating temperature causes oxidation of a large number of  $C_2H_6O$  molecules, thus producing a very large number of electrons. Therefore, conductivity increases largely. This is the reason why the gas sensitivity increases with operating temperature. However, the sensitivity decreases at

higher operating temperature, as the oxygen adsorbents are desorbed from the surface of the sensor [35]. In addition, at a higher temperature, the carrier concentration increases due to intrinsic thermal excitation and the Debye length decreases. This may be one of the reasons for decreases gas sensitivity at higher temperature [36].

## 4 Conclusion

Based on the structural, compositional, topography, surface morphology, optical and gas sensing performance of our samples were emerge out the following points: (i) different thickness of the  $TiO_2$  films were examined by using optical profilometer and the obtained thickness are 186, 234, 311, 397, 433 nm with respect to volume proportion (ii) all samples exhibits a polycrystalline anatase phase of tetragonal structure with strong plane orientation (101), and the observed crystalline size were decreased with increase in thickness. (iii) AFM shown the average roughness value were increased by increase the thickness and the morphological behavior of micro spherical structure with reduced particle sizes as revealed in the study of FESEM. (iv). The optical transmittance values were decreased with an blue shift of absorption edge; the band values were decreased with increase in thickness due to the improvement of defect-free quality films was determined by optical measurement. (v). Finally, the gas sensing performance of  $TiO_2$  nanofilms shows their sensitivity response (%) with respect to operating temperature, coated thickness and gas concentration of various gasses. The reducing gas of  $C_2H_6O$  exhibits a greatest sensitivity response ( $S=13\%$ ) against other gasses at  $300^{\circ}C$  for 150 ppm of gas concentration.

**Acknowledgements** One of the authors (V. Gopala Krishnan) gratefully acknowledges to Dr. T. Shripathi, Dr. U. P. Deshpande and Er. Mohan Gangrade from the UGC—DAE CSR, Indore Centre, Khandwa Road, India for their scientific advice and for providing the necessary laboratory facilities such XPS and AFM measurements for carry out this investigation.

## References

1. D. Mardare, N. Iftimie, D. Luca, J. Non-Cryst. Solids **354**, 4396–4400 (2008)
2. I. Vaiciulis, M. Girtan, et al., Proc. Rom. Acad. Seri. A **13**(4), 335–342 (2012)
3. H. Ichiura, T. Kitaoka, H. Tanaka, Chemosphere **50**(1), 79–83 (2003)
4. M.O. Abou-Helal, W.T. Seeber, Appl. Surf. Sci. **195**, 53 (2002)
5. N.E. Stankova, I.G. Dimitrov, et al., Appl. Surf. Sci. **254**, 1268 (2007)
6. I. Poullos, P. Spathis, et al., J. Environ. Sci. Health. A, **34**(7), 1455–1471 (1999)
7. G.P. Burns, J. Appl. Phys. **65**, 2095 (1989)

8. H.G. Choi, S. Yong, D.K. Kim, Kor. J. Mater. Res. **22**(7), 352–357 (2012)
9. V. Gopala Krishnan, P. Elango, et al., Optik-Int. Light Electron Optics **127**, 11102–11110 (2016)
10. H. Tang, K. Prasad, et al., Sens. Actuators B Chem. **26–27**(1–3), 71–75 (1995)
11. K.L. Choy, B. Su, J. Mater. Sci. Lett. **18**, 943–945 (1999)
12. M. Bockmeyer, B. Herbig, et al., Thin Solid Film **517**, 1596–1600 (2009)
13. N. Rausch, E.P. Burte, J. Electrochem. Soc. **140**(1), 145–149 (1993)
14. J-C Orlianges, et al., J. Appl. Surf. Sci. **263**, 111–114 (2012)
15. M. Bouaicha, N. Ghrairi, Nanoscale Res. Lett. **7**, 357 (2012)
16. A.I. Martinez, et al., J. Phys. **16**(22), S2335–S2344 (2004)
17. R. Mariappan, V. Ponnuswamy, et al., Mater. Sci. Semicond. Process. **16**, 1328–1335 (2013)
18. L. Wei, O. Caiwen, P. Huang, et al., Int. J. Electrochem. Sci. **8**, 8213–8226 (2013)
19. I. Oja, A. Mere, M. Krunks, et al., Thin Solid Film **515**, 674–677 (2006)
20. F.D. Duminica, F. Maury, et al., Thin Solid Film **515**, 7732–7739 (2007)
21. H. Zabova, V. Cirkva, J. Chem. Technol. Biotechnol. **84**, 1624–1630 (2009)
22. W. Niu, G. Wang, et al., Int. J. Electrochem. Sci. **10**, 2613–2620 (2015)
23. B.D. Cullity, *Elements of X-ray Diffraction*, 2nd edn. (Addison-Wesley Publishing Company Inc, Toronto, 1978)
24. S.K. Joung, T. Amemiya, et al., Chem. Eur. J. **12**, 5526–5534 (2006)
25. M.A. Martynez, C. Guillen, J. Herrero, J. Appl. Surf. Sci. **136**, 8 (1998)
26. D. Mardare, M. Tasca, M. Delibas, et al, J. Appl. Surf. Sci. **156**, 200–206 (2000)
27. N.M. Ganesan, T.S. Senthil, et al., Int. J. Chem. Tech. Res. **6**(5), 3078–3082 (2014)
28. K.Y. Rajpure, C.D. Lokhande, et al., Mater. Res. Bull. **34**, 1079–1087 (1999)
29. A.A. Haidrya, J. Puskelova, et al., Appl. Surf. Sci. **259**, 270–275 (2012)
30. C.H. Han, D.W. Hong, et al., Sens Actuators B Chem. **128**, 320–325 (2007)
31. L.A. Patil, D.N. Suryawanshi, et al., Bull. Mater. Sci. **37**(3), 425–432 (2014)
32. C. Garzella, E. Comini, et al., Sens Actuators B Chem. **68**, 189–196 (2000)
33. P. Shailesh, C. Manik, et al., J. Sensor Technol. **1**, 9–16 (2011)
34. M.R. Vaezi, S.K. Sadrnezhad, Mater. Sci. Eng. B **140**, 73–80 (2007)
35. H. Windichamann, P. Mark, J. Electrochem. Soc. **126**(4), 627–633 (1979)
36. J. Mizsei, Sens Actuators B Chem. **23**, 173–176 (1995)